ACS OMEGA

http://pubs.acs.org/journal/acsodf

Article

Silica-Encapsulated Germania Colloids as 3D-Printable Glass Precursors

Alexandra C. Chinn, Eric L. Marsh, Tim Nguyen, Zackarea B. Alhejaj, Matthew J. Butler, Bachtri T. Nguyen, Koroush Sasan, Rebecca J. Dylla-Spears, and Joel F. Destino*

Cite This: *ACS Omega* 2022, 7, 17492−17500

Read Online

ACCESS | Metrics & More | Article Recommendations | Supporting Information

ABSTRACT: Core−shell colloids make attractive feedstocks for three-dimensional (3D) printing mixed oxide glass materials because they enable synthetic control of precursor dimensions and compositions, improving glass fabrication precision. Toward that end, we report the design and use of core−shell germania−silica (GeO_2−SiO_2) colloids and their use as precursors to fabricate GeO_2−SiO_2 glass monoliths by direct ink write (DIW) 3D printing. By this method, GeO_2 colloids were prepared in solution using sol−gel chemistry and formed oblong, raspberry-like agglomerates with ∼15 nm diameter primary particles that were predominantly amorphous but contained polycrystalline domains. An ∼15 nm encapsulating SiO_2 shell layer was formed directly on the GeO_2 core agglomerates to form core−shell GeO_2−SiO_2 colloids. For glass 3D printing, GeO_2−SiO_2 colloidal sols were formulated into a viscous ink by solvent exchange, printed into monoliths by DIW additive manufacturing, and sintered to transparent glasses. Characterization of the glass components demonstrates that the core−shell GeO_2−SiO_2 presents a feasible route to prepare quality, optically transparent low wt % GeO_2−SiO_2 glasses by DIW printing. Additionally, the results offer a novel, hybrid colloid approach to fabricating 3D-printed Ge-doped silica glass.

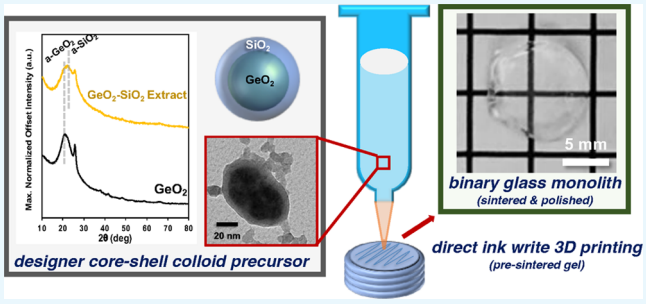

1. INTRODUCTION

Transparent inorganic glass optical materials are an essential part of everyday life and enable state-of-the-art research endeavors, from their use in smartphone cameras to NASA's Hubble Space Telescope. While glass materials are ubiquitous, conventional processing methods (i.e., melt quench fabrication) fundamentally constrain glass fabrication and formation. Unconventional approaches to making inorganic glass are vital to discovering and investigating new glass materials.[1−5]

For decades, sol−gel chemistry has been used to fabricate transparent inorganic optical coatings and glass monoliths.[6−8] In this process, molecular precursors are hydrolyzed in the presence of acid or base and then (poly)condense to form a colloidal suspension (a sol) that then sets to make a thermally treated gel to a full-density glass. Until recently, this approach was primarily limited to casting technologies, but the sol−gel process is now playing a central role in additive manufacturing (AM), three-dimensional (3D) printing, transparent glass, and glass−ceramic optical materials.[9−12]

We first reported the fabrication of optical quality silica and silica−titania glasses from sol−gel-derived colloidal feedstocks.[9] In this procedure, core−shell silica−titania nanoparticles were prepared in solution, concentrated into a viscous ink, extruded into a gel by direct ink write (DIW) AM, and thermally processed to a transparent glass optic. By synthetically tuning the composition (in weight percent titania) of the colloidal system, the refractive index of the resulting glass was readily tuned. From these feedstocks, the manufacture of DIW optical components with gradient compositions and optical properties unachievable by conventional glass fabrication processes has been realized.[12] Consequently, the design of novel 3D-printable colloidal systems is central to discovering and engineering novel and advanced transparent glass optics.

Germania (GeO_2) is an essential silica (SiO_2) glass dopant used for refractive index modification in fiber optics and waveguides.[13−16] Like SiO_2, GeO_2 is a glass network former, incorporating readily into an amorphous network composed of random (GeO_4) tetrahedra.[17] Binary silica−germania glasses exhibit low optical dispersion and the potential for second-harmonic generation.[18] SiO_2−GeO_2 glass is commonly prepared by melt quench requiring high-temperature processing of viscous molten liquids or layered structures by chemical vapor deposition, limiting glass formation and application.[19−22]

Received: April 12, 2022
Accepted: April 29, 2022
Published: May 10, 2022

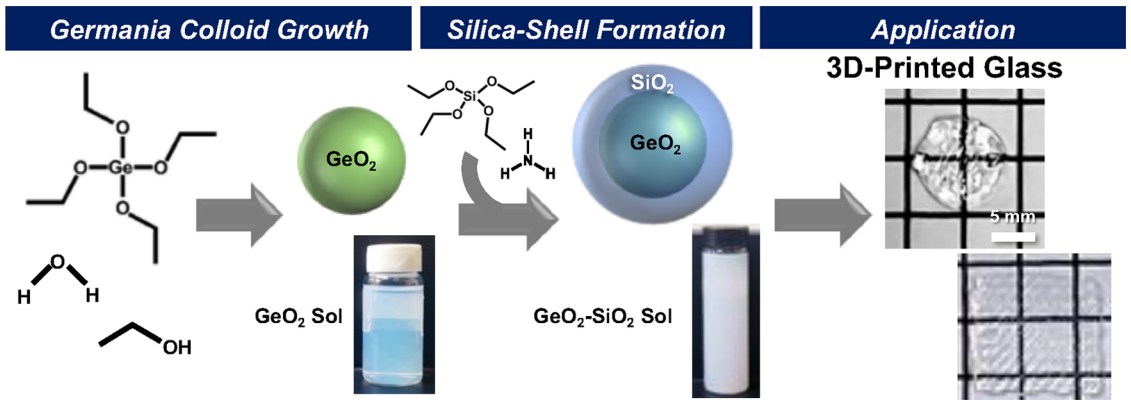

Figure 1. Overview scheme illustrating the growth of the GeO_2 core colloid, SiO_2-shell formation seeded directly on the GeO_2 surface, and the application of the hybrid colloid feedstock for the fabrication of 3D-printed SiO_2−GeO_2 glass. Photographs of an actual GeO_2 colloid sol, core−shell GeO_2−SiO_2 colloid sol, and fully sintered 2.5 wt % GeO_2−SiO_2 3D-printed glasses prepared from a GeO_2−SiO_2 colloid sol are included.

Sol−gel formation of silica−germania glasses and thin films has been previously reported by cohydrolyzing germanium and silicon alkoxide precursors under acidic conditions.[23−25] However, this approach is typically limited to casting-type applications as sols rapidly undergo gelation to form an extended oxide network, instead of stable colloidal sols. Furthermore, with cohydrolysis of Ge- and Si-alkoxide mixtures, the control of compositional speciation is limited.[26]

Recently, we reported the formation of DIW SiO_2−GeO_2 glass via mixing independent SiO_2 and GeO_2 sols to prepare an ink with variable compositions and glasses with variable refractive indices.[27] Here, we introduce an alternative approach centered on the design of core−shell GeO_2−SiO_2 colloids and their use to fabricate 3D-printed transparent glass. The fundamental difference in this approach is that a hybrid, core−shell motif is used, which could allow for the improved control of compositional speciation at the nanoscale. Another potential benefit is that encapsulating the hygroscopic and slightly water-soluble germania core particle[28] with a covalently bound silica shell could improve material durability at various stages of fabrication. Toward realizing those advantages, we report the synthesis and characterization of sols comprised of core−shell GeO_2−SiO_2 colloids and demonstrate their use in application as glass precursor to fabricate low wt % GeO_2-doped silica glass by DIW 3D printing. An introductory overview of the reported process is illustrated in Figure 1.

2. EXPERIMENTAL SECTION

2.1. Sample Preparation. *2.1.1. Core−Shell GeO_2−SiO_2 Colloid Synthesis.* Germania sols were prepared by mixing ethanol (200 Proof ACS/USP grade), water (nanopure, 18.2 MΩ cm), and tetraethoxygermane (TEOG) (Gelest) in a 112.50:12.50:1.00 mole ratio and then stirred while heating at 50 °C for 6 h under ambient conditions. A typical germania sol (theoretical yield of 0.25 g GeO_2) was prepared by mixing 0.53 mL of TEOG with 15.69 mL of ethanol and 0.54 mL of water. A photograph of the typical GeO_2 sol is shown in Figure 1.

A silica shell was added to the germania core particles in the desired glass dopant concentrations (2.5 and 5.0 wt % GeO_2). The silica sol was prepared by mixing ethanol (200 Proof ACS/USP grade), water (nanopure, 18.2 MΩ cm), ammonia (from 14.8 M NH_4OH), and tetraethoxysilane (TEOS) (Alfa Aesar, 99+%) in a 16.42:2.57:0.13:1.00 ratio. For example, a typical silica sol (theoretical yield of 9.75 g SiO_2) was prepared by mixing 36.2 mL of TEOS with 155.6 mL of ethanol, 6.00 mL of water, and 1.54 mL of ammonia solution. Upon combining the components of the silica sol, the germania sol (as described vide supra) was added dropwise for 3 min while stirring to prepare a 2.5 wt % GeO_2−SiO_2 sol. The resulting sol was then aged for a minimum of 5 days. The same procedure was followed to prepare the 5.0 wt % GeO_2−SiO_2 sols, except with twice the amount of GeO_2 sol, and a SiO_2 sol prepared from 35.3 mL of TEOS, 151.2 mL of ethanol, 5.28 mL of water, and 1.50 mL of ammonia solution. A photograph of a typical 2.5 wt % GeO_2−SiO_2 sol is shown in Figure 1.

2.1.2. Ink Formulation and DIW Fabrication. Inks were prepared by a one-pot solvent exchange method following a procedure described previously.[9,27] In brief, low-vapor-pressure solvents, tetraethylene glycol (TG) dimethyl ether, propylene carbonate (PC), and 1-hexanol were added to the GeO_2−SiO_2 sol. Ethanol, ammonia, and water were removed by rotary vacuum evaporation. A typical ink contained 9.63 g of PC, 8.75 g of TG, 0.34 g of 1-hexanol, and 10.0 g of GeO_2−SiO_2 solids. Upon evaporation, the viscous ink exhibited a shear-thinning viscoelastic response comparable to previous DIW glass slurry formulations.[9,27] The inks were next loaded into a 10 mL syringe barrel, centrifuged at 1500 rpm for 5 min, and printed using a modified commercial 3D printer (Ultimaker 2+) and a syringe pump (WPI, AL-1000HP) and printed onto a silicone baking mat used as a substrate. Linear flow rates were typically maintained at 5 mm/s, and the printed parts presented were fabricated with a 15 gauge or 1.4 mm nozzle (Nordson EFD). Figure 2A includes an image of the DIW/3D-printed monolith designed in TinkerCad and sliced in CURA. Figure 2B shows a photograph of the modified Ultimaker 2+ with a syringe pump that extrudes from the syringe into a Tygon R-3603 tubing and out the nozzle mounted using a 3D-printed holder (Structur3D). A photo of a print session is provided in Figure 2C.

2.1.3. Thermal Processing. DIW monolithic forms were allowed to dry in a desiccator cabinet for a minimum of 5 d and then released from the silicone substrate. The parts were then heated to remove organic components and sintered to full densification. Thermal processing in a small box furnace (MTI Corp., KSL-1200X) included a ramp to 300 °C at 0.1 °C/min, a dwell at 300 °C for 120 min, a ramp to 500 °C at 1.0 °C/min, and a final dwell at 500 °C for 120 min before a return to ambient temperature at a rate of 0.5 °C/min. Organic-free monoliths are stored in a desiccator cabinet before high-temperature sintering, including a ramp to 1100 °C at 4 °C/

https://doi.org/10.1021/acsomega.2c02292
ACS Omega 2022, 7, 17492−17500

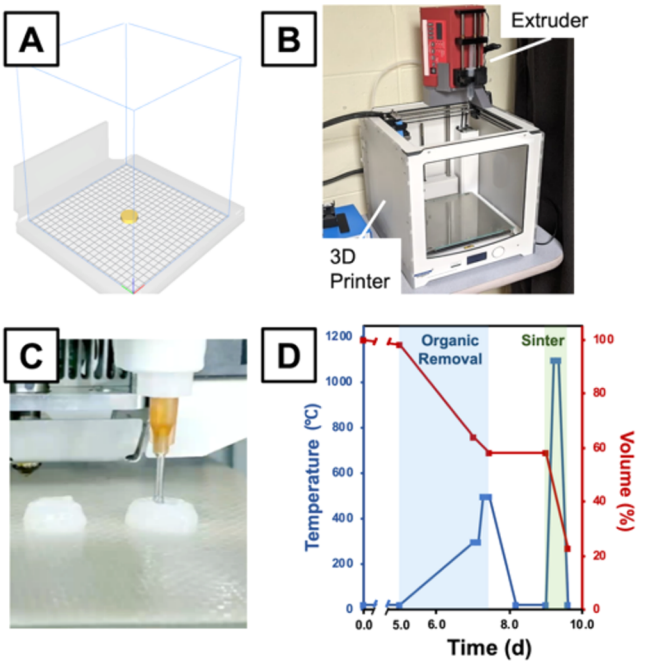

Figure 2. Fabrication of 3D-printed glass monoliths. (A) Forms were designed using commercial software and (B) printed using a commercial printer modified with a syringe pump to extrude the shear-thinning, viscous ink containing ∼35 wt % solids (i.e., GeO_2−SiO_2 colloids). (C) An example of a typical printed monolith extruding from a 1.4 mm nozzle. Printed parts are dried, and organic solvents are removed and sintered following the thermal profile shown (D); the corresponding volumetric shrinkage as a function of temperature is also shown.

min and a dwell at 1100 °C for 90 min. A graph of the thermal treatment and volumetric change profile is shown in Figure 2D. As typical of sol−gel-to-glass conversion, the large volumetric changes can result in cracking.[29,30] For these materials, this is particularly the case early during the organic removal stage, while the gel builds network strength, transforming to a xerogel. For this method, a 30 ± 10% yield of fully dense, intact (uncracked) glass was observed.

2.2. Sample Characterization. *2.2.1. GeO_2 and GeO_2−SiO_2 Colloid Analysis.* Colloid size and morphology were characterized by electron microscopy. Transmission electron micrographs were acquired with an FEI Tecnai G2 Spirit operating at an accelerating voltage of 120 kV. Samples were prepared by diluting 100-fold using HPLC-grade methanol (Fisher Scientific) onto an ultrathin carbon film with a lacy carbon support Cu mesh (Ted Pella) and dried under ambient conditions. Colloid dimensions were measured using the FIJI "Analyze Particles" tool.[31] Scanning electron micrographs were acquired with a Thermo Scientific Phenom Pharos Desktop SEM equipped with a field emission source at 15 kV using backscattered electron and secondary electron detectors. Samples were mounted using conductive carbon tabs (Ted Pella) and imaged directly.

Colloid chemistry and structure were characterized by vibrational spectroscopy and X-ray techniques. Attenuated total internal reflectance Fourier-transform infrared spectroscopy (ATR-FTIR) spectra were acquired on a ThermoFisher Nicolet iS10 spectrometer, equipped with a diamond crystal attachment. Sols were dropcast directly on the ATR crystal, and the water and solvent were allowed to evaporate under ambient conditions (typically, <1 min). Raman spectra were acquired on a Bruker Senterra II confocal Raman microscope equipped with a 785 nm excitation laser, a 50x objective, and a 1200 groove/mm grating (spectral resolution of 3−5 cm^{-1}). Survey X-ray photoelectron spectroscopy (XPS) measurements were acquired using a Thermo Scientific K-Alpha+ XPS (Al Kα with an energy of 1486.6 eV) with a pass energy of 200 eV. An Ar ion beam was used to remove ∼10−20 nm of material to characterize the chemical structure throughout the core−shell particles. X-ray diffraction (XRD) measurements were acquired with a PANalytical Empyrean diffractometer equipped with a Cu anode operated at 45 kV and 40 mA. Samples were deposited onto a zero diffraction Si sample holder. Where noted, core−shell GeO_2−SiO_2 colloids were extracted from their parent sol by centrifugation at 15 000 rpm for 2 min. The larger core−shell particles formed a solid compact that was recovered and resuspended in ethanol (to ∼5 wt % solids) for further analysis, while the smaller, free SiO_2 colloids remained suspended in the decanted supernatant solution.

2.2.2. Germania−Silica Glass Analysis. Glass surface morphology, microstructure, and elemental composition from Figure 6 were characterized by scanning electron microscopy using an FEI Quanta 200 SEM at 15 kV equipped with a Bruker AXS Quantax XFlash 4010 X-ray microanalysis detector for energy-dispersive X-ray spectroscopy (EDS). Sintered glass samples were mounted using conductive carbon paste and sputter-coated with ∼5 nm of Au/Pd. ATR-FTIR spectra were acquired on a ThermoFisher Nicolet iS10 spectrometer, equipped with a diamond crystal attachment. Sintered glass samples were nondestructively analyzed using a standard anvil to hold the glass to the diamond crystal surface. XRD measurements were acquired with a PANalytical Empyrean diffractometer equipped with a Cu anode operated at 45 kV and 40 mA. Samples were ground for analysis using an agate mortar and pestle and deposited onto a zero diffraction Si sample holder. UV−vis transmission spectra were acquired on an Agilent Cary 300 double-beam spectrophotometer. DIW glass samples were ∼2 mm thick. The refractive index was measured using a Metricon model 2010 prism coupler at 377, 532, and 1061 nm. Dispersion values were modeled from a Cauchy fit. Optical measurements were acquired on polished samples.

3. RESULTS AND DISCUSSION

In contrast to sol−gel-derived SiO_2, which is well known to form stable, spherical, amorphous colloidal suspensions, or sols, reports of sol−gel-derived GeO_2 sols describe the formation of crystalline and polycrystalline materials.[32,33] The tendency for GeO_2 to form crystalline domains can be attributed to the presence of water in the solution, which is critical for alkoxide hydrolysis but also produces favorable chemical kinetics through a chemical dissolution pathway that promotes crystallization from GeO_2 glass, even at ambient conditions.[34] Aware of these challenges, a GeO_2 sol formulation was developed from a systematic study of TEOG-derived sols by varying reaction conditions, such as water stoichiometry, use of a catalyst, and reaction temperature. The synthesis presented produced stable and minimally crystalline GeO_2 core colloids with a low water stoichiometry. SiO_2 encapsulation was achieved using a Stöber silica formulation adapted from previous reports.[9,27,35] In this synthesis, silica growth is seeded directly on the GeO_2 colloid

https://doi.org/10.1021/acsomega.2c02292
ACS Omega 2022, 7, 17492−17500

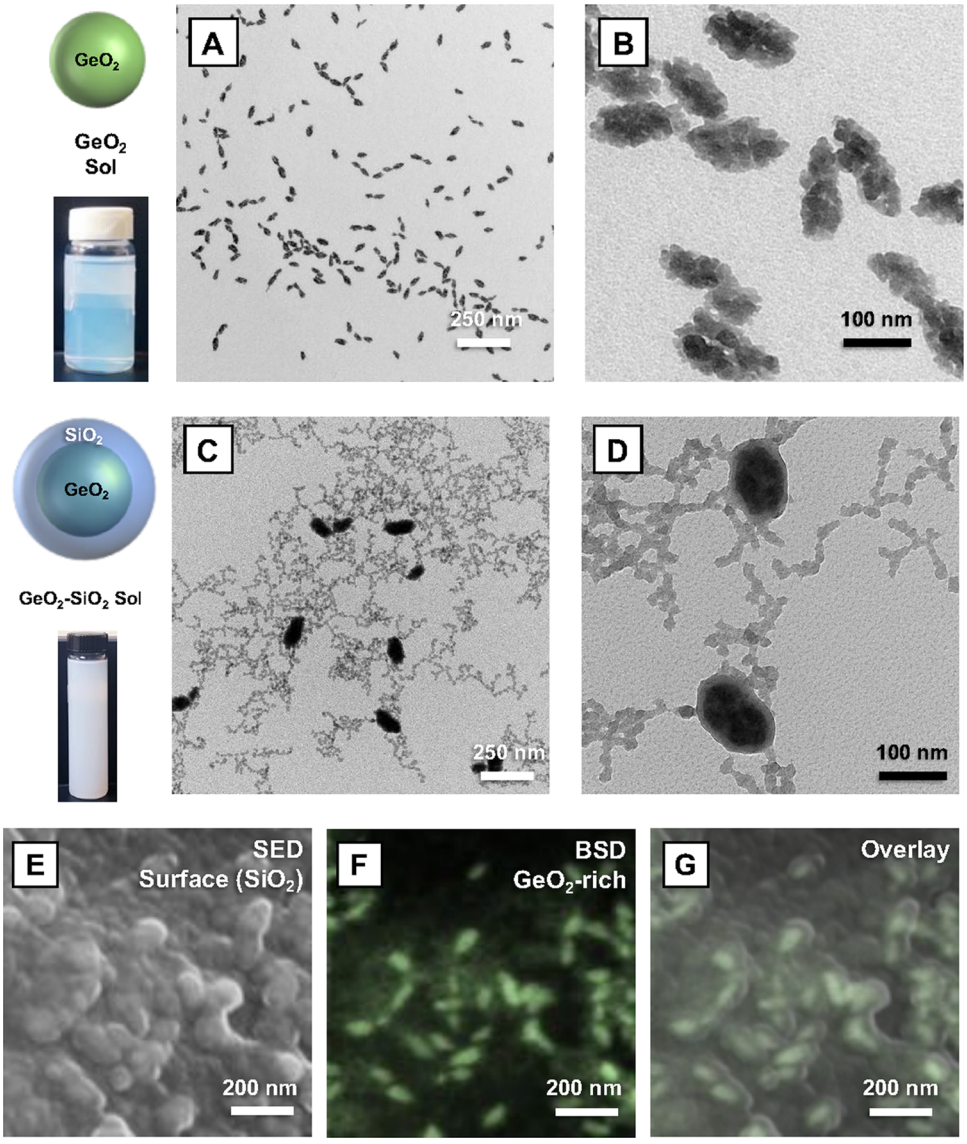

Figure 3. Electron micrographs of individual and core−shell colloids. (A, B) GeO_2 colloid transmission electron micrographs. (C, D) Transmission electron micrographs of SiO_2-encapsulated GeO_2 colloids (from a 5 wt % GeO_2 sol), along with independent SiO_2 colloids formed in solution. Scanning electron micrographs of core−shell GeO_2−SiO_2 colloids (from a 5 wt % GeO_2 sol) acquired with (E) a secondary electron detector (SED), (F) a backscattered electron detector (BSD), and (G) a semitransparent overlay of the two micrographs to show contrast and SiO_2 shell thickness.

and linked by condensation reactions with reactive surface hydroxides. Hybrid silica-metal/semimetal oxide nanostructures and encapsulation strategies utilizing this chemistry have been reported extensively.[36−40] However, this is believed to be the first report in use for forming core−shell GeO_2−SiO_2 colloids.

Figure 3 presents electron micrographs of the GeO_2 core and the core−shell GeO_2−SiO_2 colloids. Figure 3A,B shows that the GeO_2 core colloids have an ellipsoidal raspberry morphology comprised of many agglomerated, spherical primary particles of ∼15 nm in diameter. Image analysis of the TEM shown in Figure 3A determined that the mean particle length and width of the oblong agglomerates were 84 (±26) and 39 (±13) nm (n = 184), respectively, approximately a 2:1 aspect ratio. Figure 3C,D shows that the germania colloids encapsulated with SiO_2 retained the ellipsoidal shape even in the core−shell motif, and free silica particles were also present in the sol, as expected due to the low wt % doping of GeO_2. Image analysis of a lower-magnification TEM of the same sample shown in Figure 3C (shown in the Supporting Information, Figure S1) determined that the mean particle length and width were 112 (±37) and 61 (±15) nm (n = 215), respectively, slightly reducing the aspect ratio with the addition of an ∼15 nm SiO_2 shell. The free SiO_2 colloids were spherical and were also ∼15 nm in diameter. Figure 3E,F shows colocalized micrographs of the core−shell colloids imaged using an SED and BSD. Since secondary electrons originate within a few nanometers of the surface, and backscattered electrons are collected from a larger volume, and larger atoms are stronger electron scatterers, the overlay image of the two signals, shown in Figure 3G, confirms the core−shell GeO_2−SiO_2 colloid motif inferred from TEM.

Structural analyses, shown in Figure 4, were conducted to probe the surface and bulk of the core and core−shell particles. ATR-FTIR data presented in Figure 4A show that the as-prepared GeO_2 exhibits a peak at 885 cm^{-1} that is broad at the

https://doi.org/10.1021/acsomega.2c02292
ACS Omega 2022, 7, 17492−17500

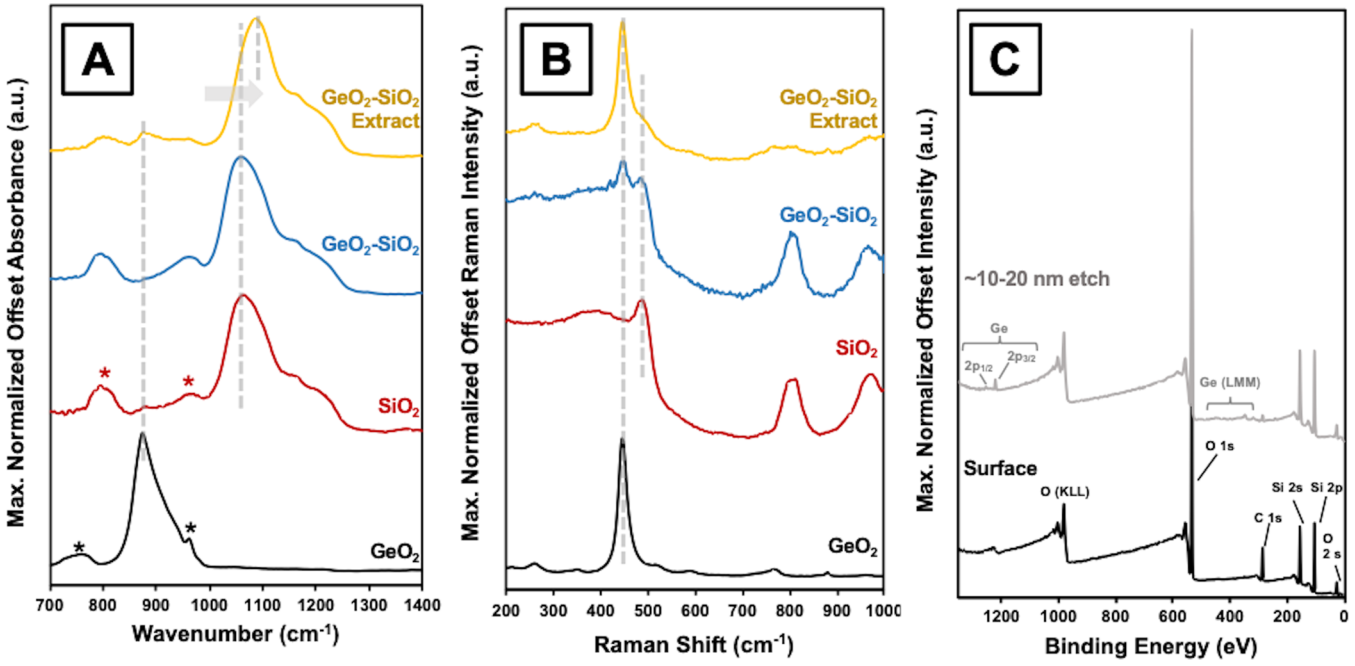

Figure 4. Structural characterization of GeO_2 and core−shell GeO_2−SiO_2 colloids. (A) ATR-FTIR and (B) Raman spectra of as-prepared GeO_2, SiO_2, core−shell GeO_2−SiO_2 (from a 2.5 wt % GeO_2 sol), and extracted (via centrifugation) core−shell GeO_2−SiO_2. (C) XPS spectra of core−shell GeO_2−SiO_2 at the sample surface and depth profiled upon the removal of ∼20 nm of material.

base with a secondary peak on the shoulder at 965 cm^{-1}. These two well-defined peaks represent asymmetric GeO_4 stretching modes associated with hexagonal GeO_2.[20,32] Given the anisotropic shape of the GeO_2 agglomerates, the presence of crystalline domains is expected. The broadness of this peak suggests some amorphous character, as well, while a broad peak at 750 cm^{-1} denotes the presence of surface hydroxyls.[34] Upon inspecting the SiO_2 and 2.5 wt % GeO_2 core−shell GeO_2−SiO_2 samples, they appear identical. Core−shell particles were extracted from the 2.5 wt % GeO_2 sol by centrifugation to elucidate their structure in the absence of free silica. Comparing the SiO_2 spectra to that of the extracted core−shell GeO_2−SiO_2 colloids shows a decrease in the symmetric Si−O stretch at 800 cm^{-1}, the asymmetric Si−OH stretch at 960 cm^{-1}, and the asymmetric siloxane stretch at 1060 cm^{-1}, all associated with the removal of free SiO_2.[41] A small but significant peak at 885 cm^{-1} signals the presence of GeO_2. A striking change is noted in the distribution of the asymmetric (1060 cm^{-1}) and symmetric siloxane stretches (1150−1200 cm^{-1}), potentially resulting from the covalent linkage of SiO_2 to the GeO_2 core colloid. Raman spectroscopy data are shown in Figure 4B, which largely echo the conclusions drawn from ATR-FTIR, with the GeO_2 exhibiting an intense peak at 445 cm^{-1}, characteristic of the symmetric Ge−O−Ge stretching in the hexagonal GeO_2.[21] This peak also appears in the as-prepared 2.5 wt % GeO_2 core−shell GeO_2−SiO_2 sample as well as in the extract. XPS analysis was conducted to chemically confirm the GeO_2−SiO_2 core−shell structure. Survey scans presented in Figure 4C show no evidence of Ge when probing at the surface, but the Ge-specific peaks do appear upon the removal of ∼10−20 nm of material. Moreover, the position of the Ge peaks is indicative of Ge(IV) and the oxide form appears to be stoichiometrically equivalent (GeO_2).[23,42,43] Altogether, structural characterization confirms the formation of hybrid GeO_2 colloids encapsulated with the chemically bound SiO_2.

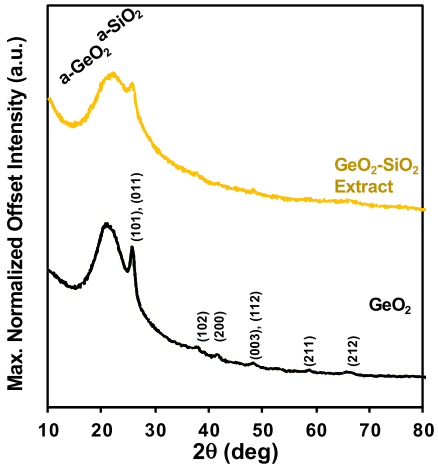

Figure 5. XRD pattern for as-prepared GeO_2 core colloids and extracted core−shell GeO_2−SiO_2 colloids.

Figure 5 includes an XRD pattern for the as-prepared core GeO_2 and extracted core−shell GeO_2−SiO_2 colloids. XRD for as-prepared GeO_2−SiO_2 colloids, including free SiO_2, was characterized at 2.5, 5, and 6 wt % but only showed a signal for amorphous SiO_2. As a result, the data is not presented. The as-prepared GeO_2 colloids exhibit broad and relatively weak peaks that are consistent with the presence of nanoscale polycrystalline domains.[33] Evidence of polycrystalline GeO_2 is detected in the XRD pattern of the extracted core−shell particles, as noted by the appearance of the (110) and (011) peaks. Altogether, structural characterization confirms the formation of hybrid GeO_2 colloids encapsulated with the chemically bound SiO_2.

As-prepared, core−shell GeO_2−SiO_2 colloidal sols of various wt % GeO_2 were formulated into 3D-printable inks, as described (see Section 2.1.2). A photograph of a typical 2.5 wt % GeO_2−SiO_2 glass is presented in Figure 1. Figure 6A−C

https://doi.org/10.1021/acsomega.2c02292
ACS Omega 2022, 7, 17492−17500

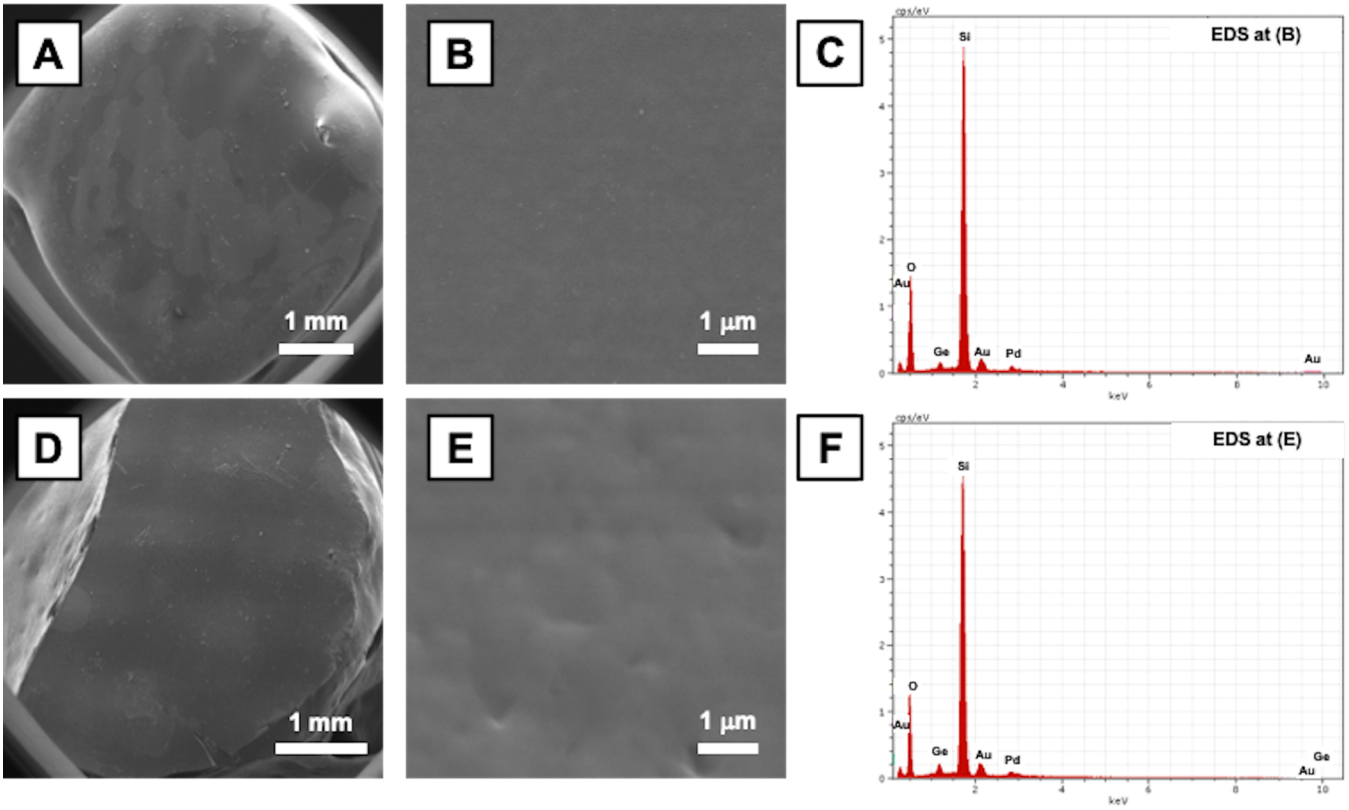

Figure 6. Physical characterization of the typical sintered 3D-printed monoliths. Scanning electron micrographs of a 3D-printed glass at low magnification and high magnification using a secondary electron detector, and energy-dispersive X-ray spectra for (A−C) 2.5 wt % GeO_2−SiO_2 and (D−F) 5.0 wt % GeO_2−SiO_2.

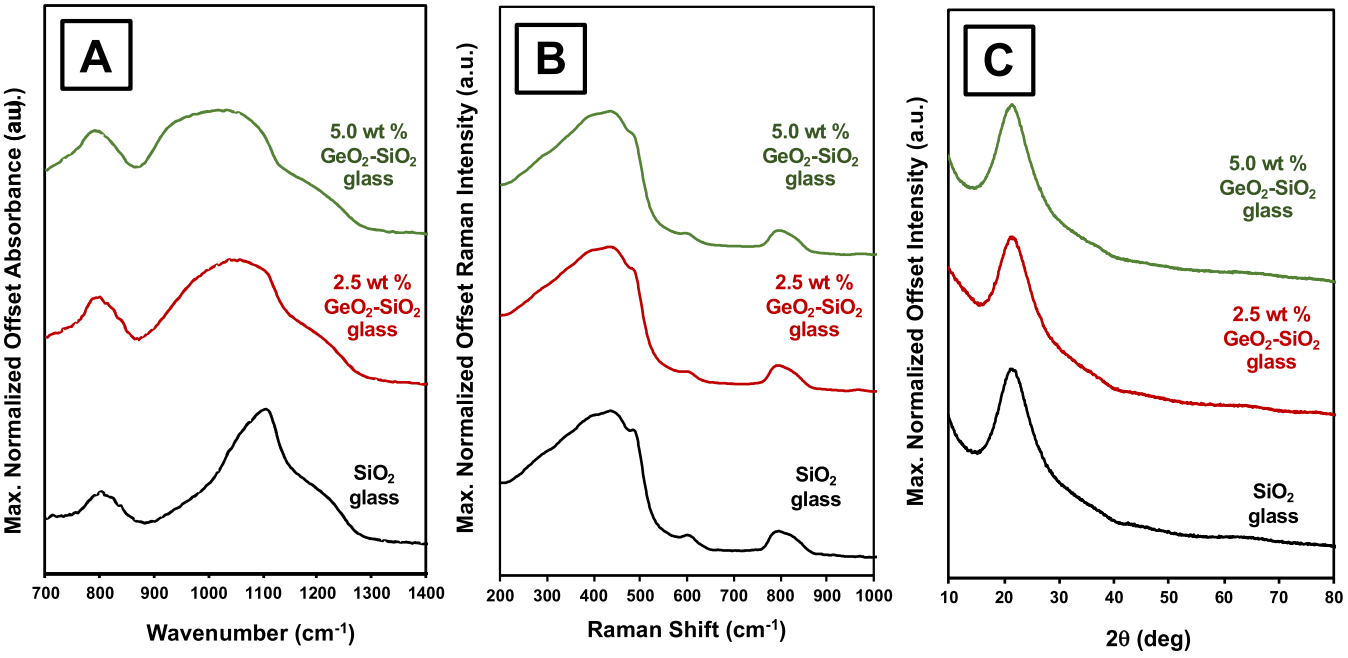

Figure 7. Structural characterization of sintered 3D-printed glasses. (A) ATR-FTIR and (B) Raman spectra of SiO_2 and 2.5 and 5 wt % GeO_2−SiO_2 glasses. (C) XRD of SiO_2 and 2.5 and 5.0 wt % GeO_2−SiO_2 glasses.

presents the characterization of a 2.5 wt % GeO_2−SiO_2 glass monolith sintered to full density. The glass surface is homogeneous, smooth, and exhibits no microscale defects or open porosity at various length scales. Elemental analysis shows the evidence of Ge, and externally calibrated quantitation results calculated 2.9 wt % GeO_2, agreeing approximately (±1%) with the expected concentration. Similarly, Figure 6D−F presents the characterization of a 5.0 wt % GeO_2−SiO_2 glass monolith. The surface appears smooth and without microstructural defects: though the high-

https://doi.org/10.1021/acsomega.2c02292
ACS Omega 2022, 7, 17492−17500

magnification micrograph shows some minor topography. The elemental analysis also confirms the presence of Ge, and quantitation results calculated 4.1 wt % GeO_2, while low, it agrees approximately with the expected concentration (within ±1%).

Structural characterization of the core−shell-colloid-derived glasses is presented in Figure 7. ATR-FTIR spectra for 2.5 wt % SiO_2 and 5.0 wt % GeO_2−SiO_2 shown in Figure 7A appear amorphous, as noted by the broadening of peaks between 900 and 1300 cm^{-1}, where the Si−O−Si and Ge−O−Ge asymmetric and symmetric stretches dominate. Raman spectra for the same samples also show a broad, amorphous peak between 100 and 550 cm^{-1}, with notably no evidence of the hexagonal GeO_2 peak previously observed at 445 cm^{-1} in the as-prepared 2.5 wt % core−shell GeO_2−SiO_2 sample. Furthermore, the "D1" and "D2" peaks associated with breathing motions for 4- and 3-membered SiO_4 rings in SiO_2 glass at 491 and 605 cm^{-1}, respectively, decrease with the addition of Ge to the glass network. This is consistent with the previous sol−gel SiO_2−GeO_2 glass reports, and it suggests Ge integration into the bulk network structure.[27,44] Lastly, XRD results for the three samples exhibit only one peak centered at 21.5° for amorphous SiO_2, confirming that the DIW glass is noncrystalline.

An example of the typical optical properties of a 3D-printed 2.5 wt % GeO_2−SiO_2 glass derived from a core−shell GeO_2−SiO_2 sol is shown in Figure 8. Figure 8A shows a photograph of the hand-polished glass optic (inset) and the UV−visible transmission spectrum for the sample. The glass exhibits ∼80−90% transmission over the visible region and decreases to ∼50% at 200 nm. Optical dispersion over the visible range was also determined for the 2.5 wt % GeO_2−SiO_2 glass sample and shows an increased refractive index in comparison to a 100% SiO_2 glass prepared by DIW.[45] At 589 nm, the refractive index was determined to be 1.461 for the 2.5 wt % GeO_2−SiO_2 compared to 1.458 for pure SiO_2.

While bulk characterization results show successful GeO_2−SiO_2 glasses 3D-printed at 2.5 and 5 wt % GeO_2, visible transmission (i.e., optical quality) variability was observed for glasses fabricated from core−shell sols with greater than 2.5 wt % GeO_2. Experimental data investigating causes of optical quality degradation in various samples is provided in the Supporting Information. Supporting results include photographs of glasses fabricated from 2.5 to 10.0 wt % GeO_2−SiO_2 sols of various optical qualities presented in Figure S2. The density and hydroxyl content for each glass are provided in Table S1. XRD analyses of those same glasses are given in Figure S3. The diffraction patterns for all of the glasses analyzed exhibit one broad peak centered at 21.5°, suggesting that the semitransparent glasses are primarily amorphous. Based on these results, the scatter loss is unlikely attributed to devitrification. BSD-SEM and EDS analyses of the semitransparent glasses prepared from 4.0, 5.0, and 8.0 wt % GeO_2−SiO_2 are provided in Figure S4. Results show that the glasses exhibit chemical speciation (i.e., heterogeneity) on the order of hundreds of nanometers to microns; given the scale, the nonuniform distribution of Ge observed may result from agglomeration of the core−shell GeO_2−SiO_2 colloids in the sol or ink formulation stages. Alternately, the heterogeneity could be related to Ge diffusion in the sintering stage. Our previous approach to sintering 3D-printed GeO_2−SiO_2 went above the melting point or liquidus temperature for GeO_2 (1116 °C) by sintering for 2 h at 1150 °C.[27,46] The GeO_2−SiO_2 glasses presented here were sintered below the melting point at 1100 °C for 2 h, ideally reducing significant diffusion to realize the benefits of the core−shell motif while enabling the structural changes necessary to achieve a densified glass network. Potentially providing evidence to counter the Ge-diffusion hypothesis, Figure S5 presents (admittedly rare) examples of relatively transparent glasses fabricated from 4.0, 5.0, and 6.0 wt % core−shell GeO_2−SiO_2 sols sintered using the same protocol as the semitransparent samples. BSD-SEM and EDS analyses of the transparent glasses show the samples to be relatively homogeneous compared to those shown in Figure S4. Additional studies are ongoing, investigating the glass network formation in core−shell-derived GeO_2−SiO_2 glasses, sintering kinetics, and optical quality variability.

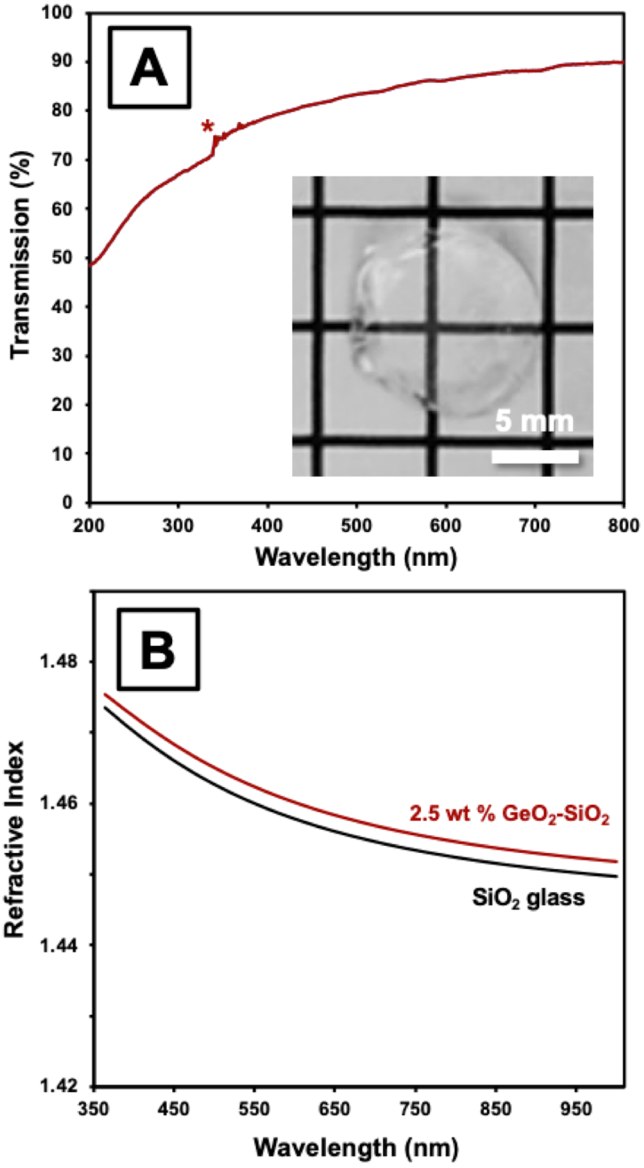

Figure 8. Optical characterization of a typical sintered 3D-printed monolith. (A) UV−visible transmission and (B) bulk optical dispersion curve for a 2.5 wt % GeO_2−SiO_2 glass, with a photograph of the polished glass (inset). The dispersion curve for DIW additively manufactured optical quality SiO_2 is included for comparison. The asterisk (*) in panel (A) denotes the position of the lamp change within the spectrometer.

https://doi.org/10.1021/acsomega.2c02292
ACS Omega 2022, 7, 17492−17500

4. CONCLUSIONS

We describe the growth of SiO_2-encapsulated GeO_2 colloids using sol−gel chemistry and their use to fabricate 3D-printed GeO_2−SiO_2 glasses. Structural analysis of the core and core−shell colloids showed that the GeO_2 used contained polycrystalline nanodomains and that the silica encapsulation layer was covalently bonded to the GeO_2 surface and formed an ∼15 nm shell. These materials were successfully used as precursor particles to fabricate low-weight-percent (2.5 and 5 wt %) GeO_2−SiO_2 glasses, as shown by ATR-FTIR, Raman, XRD, and electron microscopy. Further, the optical characterization of an example 2.5 wt % GeO_2−SiO_2 glass showed good transmission over the UV−visible range and an increased refractive index compared to that of the 100% SiO_2 glass. Ongoing research seeks to better understand the sources of optical quality variation in higher (4.0−10.0) wt % GeO_2 glasses and explore the design of other, novel DIW colloidal feedstocks that enable the study of glass materials unachievable by conventional melt quench processes.

■ ASSOCIATED CONTENT

Supporting Information

The Supporting Information is available free of charge at https://pubs.acs.org/doi/10.1021/acsomega.2c02292.

Sample electron micrograph of core−shell colloids analyzed for measuring particle dimensions (Figure S1); photographs of polished, 2.5−10 wt % GeO_2−SiO_2 glasses (Figure S2); XRD of opaque/semitransparent 4−10 wt % GeO_2−SiO_2 glasses (Figure S3); physical characterization of opaque/semitransparent, sintered 4.0, 5.0, and 8.0 wt % GeO_2−SiO_2 3D-printed glass monoliths (Figure S4); physical characterization of transparent, sintered 4.0, 5.0, and 6.0 wt % GeO_2−SiO_2 3D-printed glass monoliths (Figure S5); and properties of DIW GeO_2−SiO_2 glasses derived from core−shell GeO_2−SiO_2 sols (Table S1) (PDF)

■ AUTHOR INFORMATION

Corresponding Author

Joel F. Destino − *Department of Chemistry & Biochemistry, Creighton University, Omaha, Nebraska 68178, United States;* orcid.org/0000-0001-8100-027X; Email: joeldestino@creighton.edu

Authors

Alexandra C. Chinn − *Department of Chemistry & Biochemistry, Creighton University, Omaha, Nebraska 68178, United States*

Eric L. Marsh − *Department of Chemistry & Biochemistry, Creighton University, Omaha, Nebraska 68178, United States*

Tim Nguyen − *Department of Chemistry & Biochemistry, Creighton University, Omaha, Nebraska 68178, United States*

Zackarea B. Alhejaj − *Department of Chemistry & Biochemistry, Creighton University, Omaha, Nebraska 68178, United States; Omaha North High Magnet School, Omaha, Nebraska 68111, United States*

Matthew J. Butler − *Department of Chemistry & Biochemistry, Creighton University, Omaha, Nebraska 68178, United States*

Bachtri T. Nguyen − *Department of Chemistry & Biochemistry, Creighton University, Omaha, Nebraska 68178, United States;* orcid.org/0000-0002-9222-8787

Koroush Sasan − *Materials Science Division, Lawrence Livermore National Laboratory, Livermore, California 94550, United States;* orcid.org/0000-0002-5577-8894

Rebecca J. Dylla-Spears − *Materials Science Division, Lawrence Livermore National Laboratory, Livermore, California 94550, United States*

Complete contact information is available at: https://pubs.acs.org/10.1021/acsomega.2c02292

Author Contributions

The manuscript was written through contributions of all authors. All authors have given approval to the final version of the manuscript.

Funding

This work was supported by the Nebraska EPSCoR First Award, the Research Corporation for the Advancement of Science, Cottrell Scholar Award, and in part under the auspices of the U.S. Department of Energy by Lawrence Livermore National Laboratory under Contract DE-AC52-07NA27344 within the LDRD program 16-SI-003. Release: LLNL-JRNL-832069. The authors thank the Creighton Haddix STEM Corridor program for supporting the research of Z.B.A., and NASA Nebraska EPSCoR for supporting the research of A.C.C.

Notes

The authors declare no competing financial interest.

■ ACKNOWLEDGMENTS

XRD and XPS experiments were performed at the Nebraska Nanoscale Facility: National Nanotechnology Coordinated Infrastructure and the Nebraska Center for Materials and Nanoscience, which are supported by the National Science Foundation under Award ECCS: 2025298, and the Nebraska Research Initiative. The Thermo Phenom Pharos SEM was acquired through a Nebraska EPSCoR MRI award to J.F.D.

■ REFERENCES

(1) Weber, J. K. R. The Containerless Synthesis of Glass. *Int. J. Appl. Glass Sci.* **2010**, *1*, 248−256.

(2) Kotz, F.; Arnold, K.; Bauer, W.; Schild, D.; Keller, N.; Sachsenheimer, K.; Nargang, T. M.; Richter, C.; Helmer, D.; Rapp, B. E. Three-Dimensional Printing of Transparent Fused Silica Glass. *Nature* **2017**, *544*, 337−339.

(3) Datsiou, K. C.; Saleh, E.; Spirrett, F.; Goodridge, R.; Ashcroft, I.; Eustice, D. Additive Manufacturing of Glass with Laser Powder Bed Fusion. *J. Am. Ceram. Soc.* **2019**, *102*, 4410−4414.

(4) Moore, D. G.; Barbera, L.; Masania, K.; Studart, A. R. Three-Dimensional Printing of Multicomponent Glasses Using Phase-Separating Resins. *Nat. Mater.* **2020**, *19*, 212−217.

(5) Dylla-Spears, R. Preshaping Clear Glass at Low Temperatures. *Science* **2021**, *372*, 126−127.

(6) Brinker, C. J.; Scherer, G. W. Sol → Gel → Glass: I. Gelation and Gel Structure. *J. Non-Cryst. Solids* **1985**, *70*, 301−322.

(7) Brinker, C. J.; Scherer, G. W. *Sol−Gel Science: The Physics and Chemistry of Sol-Gel Processing*, Academic Press: Boston, MA, 1990.

(8) Ciriminna, R.; Fidalgo, A.; Pandarus, V.; Béland, F.; Ilharco, L. M.; Pagliaro, M. The Sol-Gel Route to Advanced Silica-Based Materials and Recent Applications. *Chem. Rev.* **2013**, *113*, 6592−6620.

(9) Destino, J. F.; Dudukovic, N. A.; Johnson, M. A.; Nguyen, D. T.; Yee, T. D.; Egan, G. C.; Sawvel, A. M.; Steele, W. A.; Baumann, T. F.;

Duoss, E. B.; Suratwala, T.; Dylla-Spears, R. 3D Printed Optical Quality Silica and Silica−Titania Glasses from Sol−Gel Feedstocks. *Adv. Mater. Technol.* **2018**, *3*, No. 1700323.
(10) Cooperstein, I.; Shukrun, E.; Press, O.; Kamyshny, A.; Magdassi, S. Additive Manufacturing of Transparent Silica Glass from Solutions. *ACS Appl. Mater. Interfaces* **2018**, *10*, 18879−18885.
(11) Gailevičius, D.; Padolskytė, V.; Mikoliūnaitė, L.; Šakirzanovas, S.; Juodkazis, S.; Malinauskas, M. Additive-Manufacturing of 3D Glass-Ceramics down to Nanoscale Resolution. *Nanoscale Horiz.* **2019**, *4*, 647−651.
(12) Dylla-Spears, R.; Yee, T. D.; Sasan, K.; Nguyen, D. T.; Dudukovic, N. A.; Ortega, J. M.; Johnson, M. A.; Herrera, O. D.; Ryerson, F. J.; Wong, L. L. 3D Printed Gradient Index Glass Optics. *Sci. Adv.* **2020**, *6*, No. eabc7429.
(13) Bellman, R. A.; Bourdon, G.; Alibert, G.; Beguin, A.; Guiot, E.; Simpson, L. B.; Lehuede, P.; Guiziou, L.; LeGuen, E. Ultralow Loss High Delta Silica Germania Planar Waveguides. *J. Electrochem. Soc.* **2004**, *151*, G541.
(14) Dianov, E. M.; Mashinsky, V. M. Germania-Based Core Optical Fibers. *J. Lightwave Technol.* **2005**, *23*, 3500−3508.
(15) Harshavardhan Reddy, P.; Kir'yanov, A. V.; Dhar, A.; Das, S.; Dutta, D.; Pal, M.; Barmenkov, Y. O.; Minguella-Gallardo, J. A.; Bhadra, S. K.; Paul, M. C. Fabrication of Ultra-High Numerical Aperture GeO_2-Doped Fiber and Its Use for Broadband Supercontinuum Generation. *Appl. Opt.* **2017**, *56*, No. 9315.
(16) Couture, N.; Ostic, R.; Reddy, P. H.; Kar, A. K.; Paul, M. C.; Menard, J. M. Polarization-Resolved Supercontinuum Generated in a Germania-Doped Photonic Crystal Fiber. *J. Phys. Photonics* **2021**, *3*, No. 025002.
(17) Salmon, P. S.; Barnes, A. C.; Martin, R. A.; Cuello, G. J. Structure of Glassy GeO_2. *J. Phys.: Condens. Matter* **2007**, *19*, No. 415110.
(18) Mizrahi, V.; Hibino, Y.; Stegeman, G. Polarization Study of Photoinduced Second-Harmonic Generation in Glass Optical Fibers. *Opt. Commun.* **1990**, *78*, 283−288.
(19) Chen, D.-G.; Potter, B. G.; Simmons, J. H. GeO_2-SiO_2 Thin Films for Planar Waveguide Applications. *J. Non-Cryst. Solids* **1994**, *178*, 135−147.
(20) Brusatin, G.; Guglielmi, M.; Martucci, A. GeO_2-Based Sol−Gel Films. *J. Am. Ceram. Soc.* **2000**, *44*, 3139−3144.
(21) Micoulaut, M.; Cormier, L.; Henderson, G. S. The Structure of Amorphous, Crystalline and Liquid GeO_2. *J. Phys.: Condens. Matter* **2006**, *18*, R753−R784.
(22) Ballato, J.; Dragic, P. Rethinking Optical Fiber: New Demands, Old Glasses. *J. Am. Ceram. Soc.* **2013**, *96*, 2675−2692.
(23) Armelao, L.; Fabrizio, M.; Gross, S.; Martucci, A.; Tondello, E. Materials Molecularly Interconnected SiO_2-GeO_2 Thin Films: Sol-Gel Synthesis and Characterization. *J. Mater. Chem.* **2000**, *10*, 1147−1150.
(24) Kawasaki, S.; Kikuchi, C.; Okino, F.; Touhara, H. Syntheses of GeO_2-SiO_2 Glasses by the Sol-Gel Method Using GeO_2. *J. Mater. Sci. Lett.* **2000**, *19*, 11−13.
(25) Grandi, S.; Mustarelli, P.; Agnello, S.; Cannas, M.; Cannizzo, A. Sol-Gel GeO_2-Doped SiO_2 Glasses for Optical Applications. *J. Sol−Gel Sci. Technol.* **2003**, *26*, 915−918.
(26) Krishnan, V.; Gross, S.; Müller, S.; Armelao, L.; Tondello, E.; Bertagnolli, H. Structural Investigations on the Hydrolysis and Condensation Behavior of Pure and Chemically Modified Alkoxides. 2. Germanium Alkoxides. *J. Phys. Chem. B* **2007**, *111*, 7519−7528.
(27) Sasan, K.; Lange, A.; Yee, T. D.; Dudukovic, N.; Nguyen, D. T.; Johnson, M. A.; Herrera, O. D.; Yoo, J. H.; Sawvel, A. M.; Ellis, M. E.; Mah, C. M.; Ryerson, R.; Wong, L. L.; Suratwala, T.; Destino, J. F.; Dylla-Spears, R. Additive Manufacturing of Optical Quality Germania-Silica Glasses. *ACS Appl. Mater. Interfaces* **2020**, *12*, 6736−6741.
(28) Xu, M. F.; Shi, X. B.; Jin, Z. M.; Zu, F. S.; Liu, Y.; Zhang, L.; Wang, Z. K.; Liao, L. S. Aqueous Solution-Processed GeO_2: An Anode Interfacial Layer for High Performance and Air-Stable Organic Solar Cells. *ACS Appl. Mater. Interfaces* **2013**, *5*, 10866−10873.
(29) Kirkbir, F.; Murata, H.; Meyers, D.; Chaudhuri, S. R.; Sarkar, A. Drying and Sintering of Sol-Gel Derived Large SiO_2 Monoliths. *J. Sol−Gel Sci. Technol.* **1996**, *6*, 203−217.
(30) Nguyen, D. T.; Meyers, C.; Yee, T. D.; Dudukovic, N. A.; Destino, J. F.; Zhu, C.; Duoss, E. B.; Baumann, T. F.; Suratwala, T.; Smay, J. E. Dylla-Spears, R. 3D-Printed Transparent Glass. *Adv. Mater.* **2017**, *29*, No. 1701181.
(31) Schneider, C. A.; Rasband, W. S.; Eliceiri, K. W. NIH Image to ImageJ: 25 Years of Image Analysis. *Nat. Methods* **2012**, *9*, 671−675.
(32) Javadi, M.; Yang, Z.; Veinot, J. G. C. Surfactant-Free Synthesis of GeO_2 Nanocrystals with Controlled Morphologies. *Chem. Commun.* **2014**, *50*, 6101−6104.
(33) Seyyal, E.; Malik, A. Silica- and Germania-Based Dual-Ligand Sol-Gel Organic-Inorganic Hybrid Sorbents Combining Superhydrophobicity and π-π Interaction. The Role of Inorganic Substrate in Sol-Gel Capillary Microextraction. *Anal. Chim. Acta* **2017**, *964*, 96−111.
(34) Xiao, Z.; Sun, X.; Li, X.; Wang, Y.; Wang, Z.; Zhang, B.; Li, X. L.; Shen, Z.; Kong, L. B.; Huang, Y. Phase Transformation of GeO_2 Glass to Nanocrystals under Ambient Conditions. *Nano Lett.* **2018**, *18*, 3290−3296.
(35) Suratwala, T. I.; Hanna, M. L.; Miller, E. L.; Whitman, P. K.; Thomas, I. M.; Ehrmann, P. R.; Maxwell, R. S.; Burnham, A. K. Surface Chemistry and Trimethylsilyl Functionalization of Stober Silica Sols. *J. Non-Cryst. Solids* **2003**, *316*, 349−363.
(36) Mao, J.; Bai, Y.; Gu, L.; Van Aken, P. A.; Tu, M. J. Preparation and Characterization of Size-Controlled CeO_2 Nanoparticles Coated with SiO_2. *J. Nanopart. Res.* **2010**, *12*, 2045−2049.
(37) Panigrahi, S.; Bera, A.; Basak, D. Ordered Dispersion of ZnO Quantum Dots in SiO_2 Matrix and Its Strong Emission Properties. *J. Colloid Interface Sci.* **2011**, *353*, 30−38.
(38) Abbas, M.; Rao, B. P.; Islam, M. N.; Naga, S. M.; Takahashi, M.; Kim, C. Highly Stable-Silica Encapsulating Magnetite Nanoparticles (Fe_3O_4/SiO_2) Synthesized Using Single Surfactantless-Polyol Process. *Ceram. Int.* **2014**, *40*, 1379−1385.
(39) Sonmez, M.; Georgescu, M.; Alexandrescu, L.; Gurau, D.; Ficai, A.; Ficai, D.; Andronescu, E. Synthesis and Applications of Fe_3O_4/SiO_2 Core-Shell Materials. *Curr. Pharm. Des.* **2015**, *21*, 5324−5335.
(40) Fleer, N. A.; Pelcher, K. E.; Zou, J.; Nieto, K.; Douglas, L. D.; Sellers, D. G.; Banerjee, S. Hybrid Nanocomposite Films Comprising Dispersed VO_2 Nanocrystals: A Scalable Aqueous-Phase Route to Thermochromic Fenestration. *ACS Appl. Mater. Interfaces* **2017**, *9*, 38887−38900.
(41) Duran, A.; Serna, C.; Fornes, V.; Fernandez Navarro, J. M. Structural Considerations about SiO_2 Glasses Prepared by Sol-Gel. *J. Non-Cryst. Solids* **1986**, *82*, 69−77.
(42) Kibel, M. H.; Leech, P. W. X-Ray Photoelectron Spectroscopy Study of Optical Waveguide Glasses. *Surf. Interface Anal.* **1996**, *24*, 605−610.
(43) Grossi, V.; Ottaviano, L.; Santucci, S.; Passacantando, M. XPS and SEM Studies of Oxide Reduction of Germanium Nanowires. *J. Non-Cryst. Solids* **2010**, *356*, 1988−1993.
(44) Henderson, G. S.; Neuville, D. R.; Cochain, B.; Cormier, L. The Structure of GeO_2-SiO_2 Glasses and Melts: A Raman Spectroscopy Study. *J. Non-Cryst. Solids* **2009**, *355*, 468−474.
(45) Fleming, J. W. Dispersion in GeO_2−SiO_2 Glasses. *Appl. Opt.* **1984**, *23*, No. 4486.
(46) Riebling, E. F. Structure of Molten Oxides. I. Viscosity of GeO_2, and Binary Germanates Containing Li_2O, Na_2O, K_2O, and Rb_2O. *J. Chem. Phys.* **1963**, *39*, 1889−1895.

https://doi.org/10.1021/acsomega.2c02292
ACS Omega 2022, 7, 17492−17500